A Novel Bone Conduction Implant - Analog Radio Frequency Data and Power Link Design

A NOVEL BONE CONDUCTION IMPLANT - ANALOG RADIO FREQUENCY DATA AND POWER LINK DESIGN

Hamidreza Taghavi, Bo Håkansson, Sabine Reinfeldt
Chalmers University of Technology
Department of Signals and Systems, SE-412 96, Gothenburg, Sweden
taghavi@chalmers.se, boh@chalmers.se, sabine.reinfeldt@chalmers.se

ABSTRACT
This paper presents an analog radio frequency (RF) data and power link design and implementation for a novel Bone Conduction Implant (BCI). Patients who are suffering from conductive disorders and single sided deafness (SSD) cannot sometimes be rehabilitated by conventional air conduction hearing aids. Today, percutaneous Bone Anchored Hearing Aid (BAHA) is an important alternative for such patients. BAHA uses a titanium implant which penetrates the skin and can cause skin infection, skin redness and requires life-long commitment of care every day.
The BCI is designed as an alternative to the percutaneous BAHA, because it leaves the skin intact. The BCI comprises an external audio processor and an implanted unit called the BCI Bone Bridge. Sound is transmitted to the implant via an inductive RF link through the intact skin using amplitude modulation (AM). The RF link is designed to operate in critical coupling to transmit maximum power to the implant. Maximum Power Output (MPO) of the BCI was measured at 2 mm coil spacing and was found to be 105 dB relative to 1 µN at the transducer resonance frequency. The output is fairly robust in 2 mm to 6 mm skin thickness range.

KEY WORDS
Bone Conduction Implant, RF data and power link, implantable hearing devices, Bone Anchored Hearing Aid, implantable transducer.

1. Introduction

Implantable medical devices with high performance integrated electronics are used for diagnosis as well as for treatment of disorders. The development of biomedical implantable devices are closely following the developments in electronic technology and the progress in power source implantation, microelectronics, material science, biomedicine, cybernetics and related fields.

1.1 Hearing by Air and Bone Conduction

The process of hearing includes the transmission of sound energy and vibrations which finally generates the nerve impulses. In air conduction (AC) hearing, sound waves entering the ear canal are transmitted through the ear canal to the middle ear. The vibrations then deliver the sound wave pattern to the inner ear and the cochlea.
In contrast to the air conduction pathway, bone conduction (BC) hearing is the process of transmitting sound energy by vibrations through the skull or neighboring parts of the body. This results in an auditory sensation and hearing. BC hearing is the secondary auditory pathway that supplements the AC process. Main AC and BC hearing paths are illustrated in Figure 1 [1].

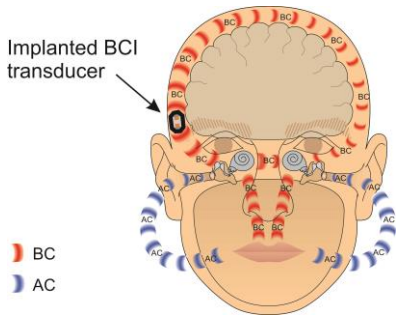

Figure 1. Bone conduction (BC) and air conduction (AC) paths: blue path represents the air conduction way from own voice, red path shows the bone conduction way of the own voice and from an implanted BCI transducer.

The main difference between hearing through AC and BC is how the cochlea receives the sound energy In BC, the bones of the skull vibrate and depending on the direction of the stimulation, the stapes remains steady or vibrates with some time lag due to its inertia. The vibrations of the skull coming from different directions vibrate the fluids in the cochlea [2].
Hearing impairment is a full or partial loss in the capability of detecting and understanding sounds which is also known as hearing loss. Hearing losses are divided into three different types dependent on their origins. These three types are: conductive loss, sensorineural loss and mixed hearing loss. Conductive hearing loss occurs when the sound is not conducted properly through the outer ear, middle ear or both. In this case, the sound still can be detected by the inner ear.

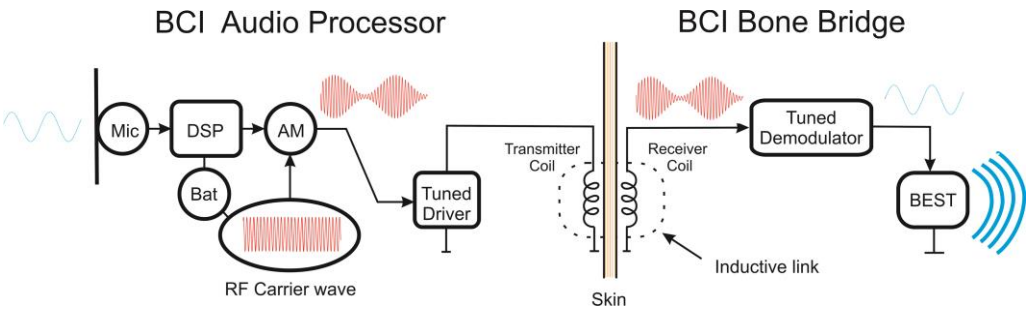

Figure 4. Principal design of the full-scale BCI device. The speech signal is picked up by the microphone (Mic) and fed to the digital signal processor (DSP). It is then transmitted through the intact skin using amplitude modulation (AM) of the radio frequency (RF) carrier wave. The speech signal is extracted by the implanted tuned demodulating unit and then is fed to the BCI transducer which uses the Balanced Electromagnetic Separation (BEST) principle.

1.2 Conventional Hearing Aids and Bone Conduction Devices

In AC hearing aids, the sound is picked up from the environment by a microphone and is fed into an amplifier or a sound processor. The amplifier will increase the intensity of the sound to a desired level and then the processed sound will drive the output transducer which is a miniaturized loudspeaker.

The BC hearing devices have the same microphone, processing and amplifier parts, but the transducer is a vibrator. In the 1980s a BC hearing aid called the Bone Anchored Hearing Aid (BAHA) was introduced [4]. The BAHA uses a titanium fixture that is anchored to the skull bone and the output transducer is attached to the implant. The sound is transmitted directly from the transducer to the skull bone. Figure 2 shows the principal design of the BAHA.

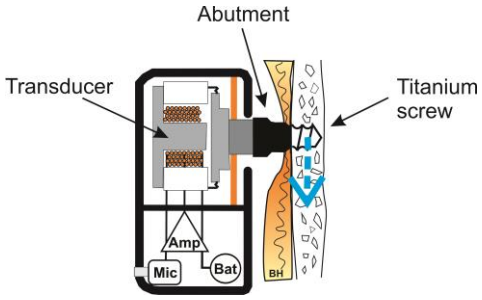

Figure 2. Principal design of a generic percutaneous Bone Anchored Hearing Aid (BAHA) with a screw attachment to the skull bone. It also comprises a microphone (Mic), battery (Bat) and pre and power amplifier (Amp) that drives the bone conduction transducer.

Patients with conductive and mixed hearing losses who cannot use an AC device are candidates for the BAHA. The BAHA has proven to be a valuable rehabilitation for these patients [5-7]. In a percutaneous BAHA, the titanium implant penetrates the skin and it requires a life-long commitment of everyday care. Complications can occur and comprise skin infections, skin redness, and risk for implant damage due to trauma [8-12]. The BAHA has also low gain margin which causes feedback problems. A solution to these drawbacks could be a novel Bone Conduction Implant (BCI). The BCI is novel because the skin is kept intact by implanting the transducer within the skull bone near to the cochlea (see Figure 3), which can also increase the sensitivity of the bone conducted sound [13-15]. There is no screw attachment to the skull bone. The BCI has an improved gain headroom than the BAHA which allows a possibility to increase the real gain of the BCI without getting feedback problems [ref feedback paper].

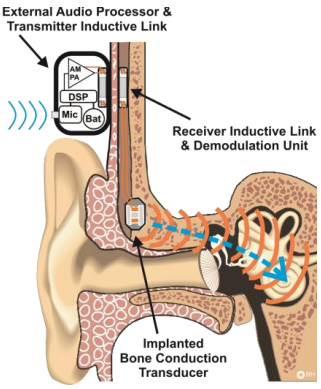

Figure 3. BCI system with an implanted and capsuled bone conduction transducer with a flat surface contact to the skull bone. It comprises also a receiver inductive link and an externally worn audio processor.

The BCI consists of an external audio processor including the microphone, digital signal processor (DSP), analog signal processing parts and the tuned power amplifier which delivers the signal and energy to an inductive RF link. The implanted part, which is called the BCI Bone Bridge, involves the receiving tuned coil, demodulator and the transducer. To transmit the signal and energy to the transducer, an amplitude modulation technique is applied. The transmitter coil and the receiver implanted

coil are aligned by a permanent magnet retention system [14]. The principal design of the full-scale BCI device is presented in Figure 4.

The aim of this study was to design the BCI device which can produce the highest output force level in the implant with a fairly robust power transmission for different skin thicknesses.

Powering the implant can be performed by using inductive RF links [16-17] or using optical methods [18]. In transcutaneous power transmission, RF links are more frequently used than optically power transmission systems. Some applications use an implanted rechargeable battery together with an internal processor and transducer. Recharging the battery can be done using optical techniques [18], inductive RF link [19], or by skin volume conduction [20]. In many applications, it is also important to send the data through the skin to the implant. In these cases, RF links can be the best choice to transmit both power and data from the same inductive link by using a modulation technique [21-23]. Since the BCI Bone Bridge contains passive components there is no need to make a regulated supply voltage for powering internal components.

2. RF Transcutaneous Power and Data Link Design

Electronic implantable devices need to be small and operate within low-power low-voltage conditions to make them portable and easy to implant. They are most often powered by inductive RF links to avoid the need for implanted batteries. Recently there is an increasing trend to make fully implantable devices where the recharging is done wirelessly trough RF links.

Figure 5 depicts the basic structure of mutually coupled coils. The self-inductances of the two coils are denoted as L_1 and L_2. The mutual inductance is denoted as M. The equations (1) and (2) explain the relations between voltages and currents.

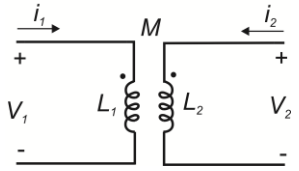

Figure 5. Mutually coupled coils with voltage and current configurations.

$$V_1 = L_1\left(\frac{di_1}{dt}\right) + M\left(\frac{di_2}{dt}\right) \quad (1)$$

$$V_2 = M\left(\frac{di_1}{dt}\right) + L_2\left(\frac{di_2}{dt}\right) \quad (2)$$

The ratio of the mutual inductance to the maximum possible value of M is called the coupling coefficient k and is expressed as:

$$k = \frac{M}{\sqrt{L_1 L_2}} \quad \text{where} \quad (3)$$

the coupling coefficient is always $0 \leq k \leq 1$.

One approach that has been presented by Hochmair [25] computes the mutual inductance based on coil geometry where cylindrical coils facing each other are considered. Solving the integrals using Bessl functions for circular (planar) coils, the mutual inductance can be calculated. To obtain the coupling coefficient, the self-inductance values are calculated by an equation from Terman [26]. The coupling formula takes also the spacing and lateral misalignment into account, but not the angular displacement. Soma *et al.* [27] introduced a formula for mutual inductance which solves the problem with complete elliptic integrals in a perfect alignment case. Also the lateral and angular misalignments were investigated. Zierhofer *et al*. [28] derived an equation for self-inductance which considers the radius of coil's wire. Combining equations in [27-28] the coupling coefficient can be computed. Both methods have been performed using MATLAB and compared to a real measurement of coils (see Figure 10).

The basic structure of an inductive RF tuned power and data link system for the BCI device is shown in Figure 6. The RF power amplifier drives the primary RF coil which sends power and data inductively across the skin of the patient to the secondary RF coil. The RF signal on the secondary side is passed through the envelop detector to extract the speech information from the RF carrier signal. Also, the power is transmitted to the load simultaneously. The power consumption of the implanted circuit is provided by an external battery that powers the primary RF coil. It is also very important for the RF link to be designed in such a manner that the amplitude of the audio signal in the secondary coil is relatively insensitive to coil separation due to the different skin thickness of patients. Also lateral misalignments must be considered. Tuning the primary and secondary coils with different methods can be performed to make the RF link to be less sensitive to spacing and lateral misalignment. There are several studies on the theoretical models and design procedures of the tuned RF links.

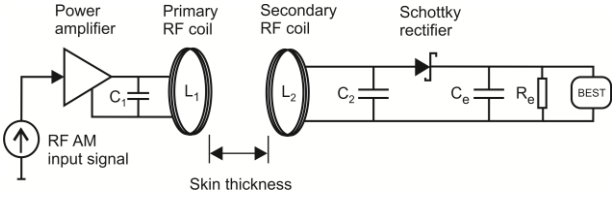

Figure 6. Basic structure of an inductive RF tuned power and data link system. The distance between capsuled coils is the skin thickness.

The most commonly used approach for the design of the inductive link is the geometric method [28-29]. It uses an external coil which is larger than the implanted coil [25,30]. The coils can move laterally, and even tilt

somewhat, with a minor effect on the gain, but it is still sensitive to the changes in the coil spacing. Ko *et al*. [30] proposed a procedure using the geometric approach for designing the transmitter and receiver coils in RF applications considering coil diameter, coil spacing, load and the number of coil turns.
They have modeled the load comprising diode and RC network by a resistor with value equal to the half of the load resistor value. In the BCI design, C_e is a part of the envelop detector and is designed to have an optimized time constant with the load resistance, so the R_L will not be half the transducer impedance magnitude. Using a shunt transmitter tuning and RF powering circuit, they designed the coils based on geometric approach. They applied shape factors of the primary and secondary coils to calculate the coupling coefficient for different geometries. According to equation (4) if the secondary diameter is d_2 and the distance between two coils is D, the primary coil diameter d_1 can be calculated to maximize the coupling between RF links

$$d_1^2 = d_2^2 + 4D^2. \qquad (4)$$

Geometric approach sacrifices the magnitude of the coupling for controlling the gain which increases the losses in the primary coil. In unequal coil size, the typical coupling coefficient is much lower than if using equally sized ones [25]. Lower coupling means that there is a need for higher current to drive the primary coil to provide the same power to the receiver. Higher current dissipates more power due to RI^2 losses in the transmitter coil.

Transcutaneous tuned RF links can be designed to operate around their critical coupling k_{crit} [16,25]. In this case, a better overall efficiency together with excellent distance tolerance can be obtained. Using two coupled tuned RF coils, the maximum secondary voltage will occur at some value of coupling coefficient which is called critical coupling. Operating near this maximum, the voltage in secondary coil will be least sensitive to changes in k. As the maximum power reaches the receiver at this peak, the efficiency will be theoretically 50% (maximum power transfer ratio in critical coupling), but there will be more losses in the secondary coil which decrease this efficiency. In this method both transmitter and receiver coils are tuned to the RF carrier signal frequency. Most common requirements need equations relating efficiency and transfer function to the coupling coefficient k. The displacement tolerance in secondary voltage depends on the rate of changes in transfer function with k [29]. The relation between transfer function and coupling efficiency is illustrated in Figure 7.
In both critical coupling and geometric approaches the transmitter and receiver coils are tuned to the carrier frequency of the circuit. The bandwidth in this design is poor and is not useful for wide bandwidth signal transmissions. Galbraith *et al.* showed a design procedure for wide-band efficient inductive transdermal power and data link with coupling insensitive gain [31].

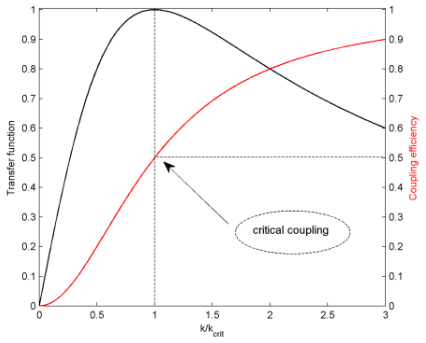

Figure 7. Critical coupling condition for coupled resonator coils in terms of gain and efficiency. Maximum output occurs in the critical coupling condition with 50% link efficiency. Transfer function and coupling coefficient are normalized.

In one version of stagger tuning (pole placement); one resonance frequency is designed to be above the carrier frequency and one below. Using this stagger tuning, the gain of the link can be desensitized from the coupling, so the coils can be separated and misaligned with little effect on the output. This design guarantees good efficiency and a large bandwidth.
In all methods the receiver coil is tuned in shunt topology because the insensitivity to distance variation increases. Also, the efficiency can be improved in this manner [29]. The primary coil can be tuned either in series or in shunt. If the primary coil is shunt tuned, then an unsaturated current source is needed to drive the RF link and a transimpedance amplifier must be designed [30].

2.1 Current-in and Voltage-out RF Link

In this topology, the primary link is tuned in shunt and is driven with an unsaturated current source. The transimpedance gain is the ratio of the voltage across the receiver coil divided by the current flowing in the transmitter coil (V_{out}/I_{in}). This determines the voltage induced in the receiver coil where the transmitter coil is driven by a current source. The saturation of the current source must be avoided. Figure 8 shows the circuit configuration of such a topology.

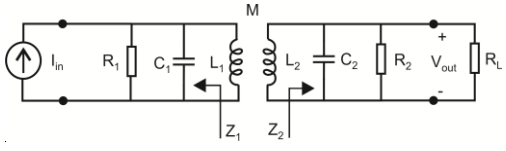

Figure 8. Current-in and Voltage-out configuration.

The transimpedance gain based on the coupling of this topology can be expressed by:

$$H(k) = \frac{j\omega k\sqrt{L_t L_r} Z_1 Z_2}{(Z_1 Z_2 + k^2\omega^2 L_t L_r - \omega^2 L_t L_r) + j(\omega L_t Z_1 + \omega L_r Z_2)} \quad (5)$$

where k is the coupling coefficient, ω is the angular frequency, L_1 is the transmitter inductance, L_2 is the receiver inductance. Z_1 and Z_2 are expressed as:

$$Z_1 = R_1 || \frac{1}{j\omega C_1} \text{ and } Z_2 = R_2 || R_L || \frac{1}{j\omega C_2} \quad (6)$$

where R_1 is the parallel resistive loss of L_1, C_1 is the transmitter tuning capacitor, R_2 is the parallel resistive loss of L_2 and C_2 is the tuning capacitor of the receiver circuit. R_L is the resistive load value which is substituted for the envelop detector network and the transducer. The critical coupling can be calculated by solving the equation below for k:

$$\frac{\partial |H(k)|}{\partial k} = 0. \quad (7)$$

This method is used for computing the critical coupling in this paper.

2.2 The Balanced Electromagnetic Separation Transducer (BEST) as Load

In this project, the goal is to deliver the energy and signal to a load which is a vibrating transducer implanted in the skull bone [34]. The transducer electrical impedance must be taken into account when designing the RF inductive link because the gain transfer function versus coupling is dependent on the load value (R_L). The load value appears in parallel with the resistive loss of the implanted coil, so it affects the gain of the transfer function and quality of the loaded secondary coil. The transducer that is used in the project is BEST90. The electrical impedance of this transducer is presented in Figure 9.

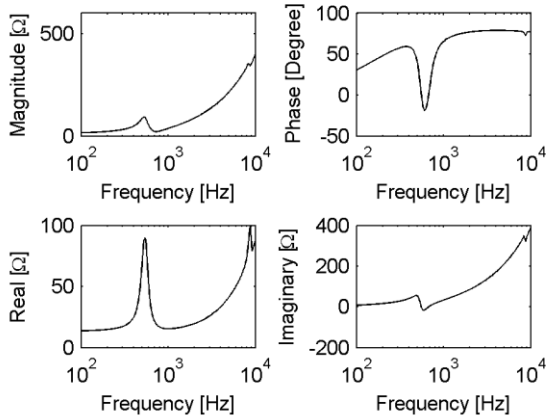

Figure 9. The electrical impedance of the BEST90 transducer. The impedance is presented as magnitude, phase, real and imaginary parts versus frequency from 100 Hz to 10 kHz.

For designing the RF link with the transducer as the load, a 50 ohm resistor was used which is equivalent to R_L at the carrier frequency. This value can reduce the quality factor of the loaded secondary coil. It is suggested that the minimum quality factor of the loaded secondary coil must not be less than 10 to minimize the power dissipation [16]. The quality factor of the loaded secondary coil in the BCI is much lower than 10 due to the 50 ohm value of the R_L and can be calculated as:

$$Q_{2,loaded} = \frac{R_2 || R_L}{\omega L_2}. \quad (8)$$

3. System Design

The aim of this paper was to design the BCI device which can generate the highest output force level with a fairly robust power transmission in the skin thickness range of 2 mm to 8 mm. Therefore the critical coupling method was applied to reach the maximum secondary voltage. Both primary and secondary coils were tuned at the carrier frequency. The transmitter coil was shunt tuned and a RF transimpedance power amplifier was designed to drive the RF link.

3.1 Coupled Resonator Design

There are limitations on the physical size of the implanted and external coils. The coupling factor range for the operation of the system can be found regarding to the lateral misalignment and coil spacing. We have chosen equally-sized circular coils with the radius of 11 mm. In most of the transcutaneous hearing implants, the skin thickness can vary from 2 mm to 8 mm. The lateral misalignment is ignored. The selected coil geometries can give a range of coupling coefficients $0.125<k<0.3$ within the required relative distance range. It was assumed that 4 mm was the optimum distance between coils which resulted in k=0.2. Based on the coil geometries and mutual inductance computations, the coupling coefficient versus coil spacing was explored. Figure 10 illustrates the coupling coefficient versus distance between two coils using two computation methods and comparing those values with the real measurements of the coils coupling coefficient. Method 1 was used by Hochmair [25] which applies Bessel functions to compute mutual inductance. Method 2 was used by Soma *et al.* [27] using Elliptic functions to solve the integrals. It can be seen that the measurements of k are in a good agreement with calculations according to method 1. Therefore this method was used to estimate the coupling coefficient in all design steps.

Based on the coupling coefficient range, the tuning of the transmitter and receiver coils was performed to operate near the critical coupling that corresponds to the optimum distance between coils. Optimized transmitter and receiver parameters were computed to explore the transimpedance transfer function versus coupling and

frequency to evaluate the performance of the RF link. Figure 11 represents the RF link transimpedance gain versus coupling coefficient. It can be seen that in the vicinity of critical coupling, variation in the coil spacing results in minor changes in the output voltage. It can also be seen that the k_{crit} occurs at a value near 0.2.

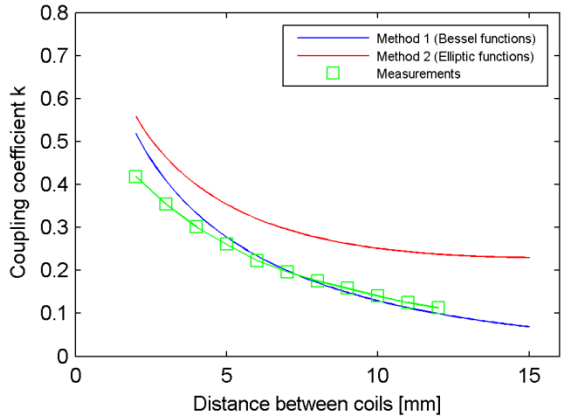

Figure 10. Coupling coefficient calculated using method 1 by Hochmair [25]; and method 2 applied by Soma *et al.* [27]. The green curve illustrates the measured coupling coefficient between coils at 10 kHz.

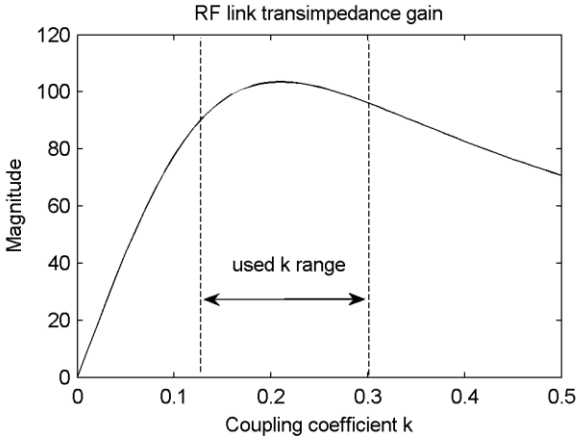

Figure 11. Transimpedance gain vs. coupling coefficient in the desired coupling range (0.125~0.3) where the transimpedance gain is optimized.

Figure 12 depicts the RF link transimpedance gain versus frequency for minimum, maximum and critical coupling factors. At the carrier frequency (normalized frequency = 1), all of the responses are nearly in their peaks, so the highest gain will be achieved. At the carrier frequency it can be seen that the gain increases by moving from maximum k to the k_{crit}, then it will decrease towards the minimum k. This is the same behavior that is expected from Figure 11.

3.2 Driver Design

In Figure 13 the analog RF power amplifier to drive the tuned RF link is presented. In this RF power amplifier, R and R' are bias resistors to bring the transistor in the boundary of cut-off and active regions. The power amplifier with LC resonant tank collector load is able to have a lower V_{CC} and less power losses than the circuits employing a resistive load at the collector. It may be shown that at the critical coupling the input resistance at the terminals of the transmitting coil decreases to the half of its value with no coupling condition (secondary coil removed).

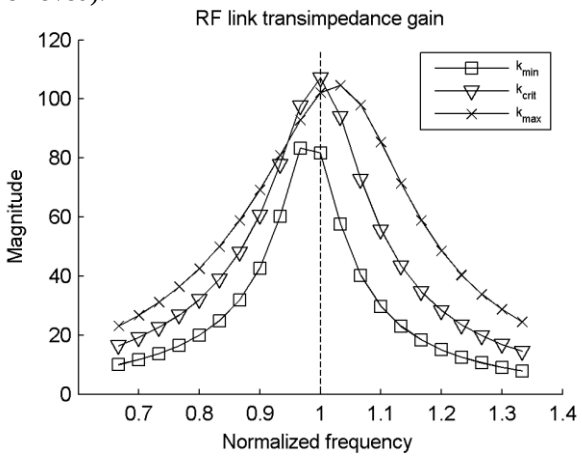

Figure 12. Transimpedance gain vs. normalized frequency in max, min and critical coupling. Maximum gain occurs in critical coupling at carrier frequency.

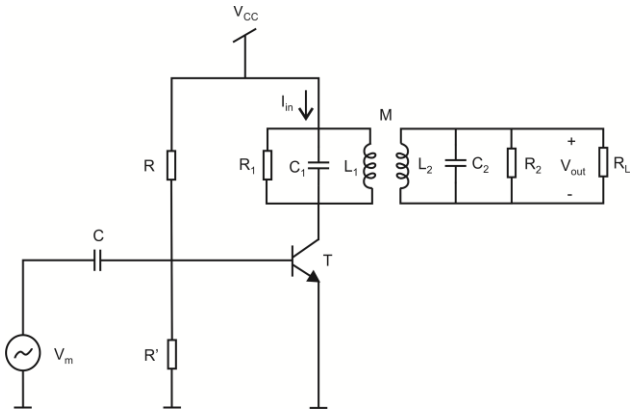

Figure 13. Analog RF power amplifier with tuned load.

Specifically, by applying a sufficiently low RF signal level to the base input, to safely prevent saturation of the transistor, the RF collector voltage of the transistor may be measured while the transmitter coil is located near the implanted receiver coil. The distance necessary for a fifty percent reduction of the RF collector voltage with respect to its value at no coupling, indicates what will be the optimum distance between transmitter and implanted coils. In this condition, the maximum secondary voltage will be applied to the implanted transducer.

3.3 Energy Efficiency

The energy transmitted from primary coil to secondary coil is dissipated in two different mechanisms. First, the energy is coupled from the primary circuit to the secondary circuit and this coupling depends on the reflected load of the secondary circuit seen from the primary circuit. Second, the energy in the receiver circuit not only dissipates in the load R_L, but it is also dissipated in the resistive loss of the receiver coil R_2. The energy delivered to the primary dissipates either in the resistive loss of the transmitter coil R_1, the rest is delivered to the secondary circuit. Typically the unloaded secondary circuit can have a high quality factor, but the overall quality factor of the secondary will be affected by the load quality factor. To achieve the minimum power dissipation in the transmitter coil, the coupling factor, quality factor of the primary circuit, and the secondary circuit quality factor need to be maximized [16].

4. Amplitude Modulation

The BCI is powered by a 1.3 VDC hearing aid battery that is used to supply the DSP, operational amplifiers, filters, AM circuit, and the power amplifier. To generate the amplitude modulation signal, a RF carrier signal was generated by an oscillator circuit. The processed sound data can be provided by low pass filtering the sigma-delta output of the DSP. Figure 14 illustrates the amplitude modulator circuit. A Junction Field Effect Transistor (JFET) is used as a Voltage Variable Resistor (VVR) with a very small drain-source voltage. Considering an N-channel JFET, the controlled voltage is provided by controlling the JFET conductance:

$$g_{DS} = \frac{2I_{DSS}}{-V_P}\left(1 - \frac{V_{GS}}{V_P}\right) \qquad (9)$$

with assumptions that

$$|V_{DS}| < 100\text{mV} \quad \text{and} \quad V_{GS} \geq V_P$$

where g_{DS} is the drain-source conductance, I_{DSS} is the drain current when $V_{GS} = 0$. V_P is the pinch-off voltage of the JFET. The constraint $|V_{DS}| < 100$ mV ensures that the JFET is operating in the ohmic (linear) region. If this JFET is applied in the input of an inverting op-amp amplifier, the output voltage will be expressed as:

$$V_m(t) = -g_{DS}\, R_f\, V_c(t) = -R_f\, \frac{2I_{DSS}}{V_P}\, \frac{V_s(t)}{V_P}\, V_c(t) \qquad (10)$$

where $V_c(t)$ is the RF carrier signal, $V_s(t)$ is the sound signal and $V_m(t)$ is the AM signal. $V_m(t)$ is proportional to the multiplication of the $V_c(t)$ and $V_s(t)$. The dynamic range of the JFET is limited, therefore to limit the distortions, $|V_{DS}| = |V_c(t)| < 100$ mV and $V_s(t)$ should be in a range that keeps the JFET in a region that transistor doesn't turn off and also not to allow the gate-source diode to be turned on. In practice a P-channel JFET was used to control the gate with a positive voltage. It can be seen in the Figure 14 that the $V_s(t)$ is coupled to the JFET by a capacitor and a DC voltage is applied to the gate to control the channel voltage to ensure a certain modulation depth. R_c and C_c are connected between gate and drain introducing a negative feedback network for linearization.

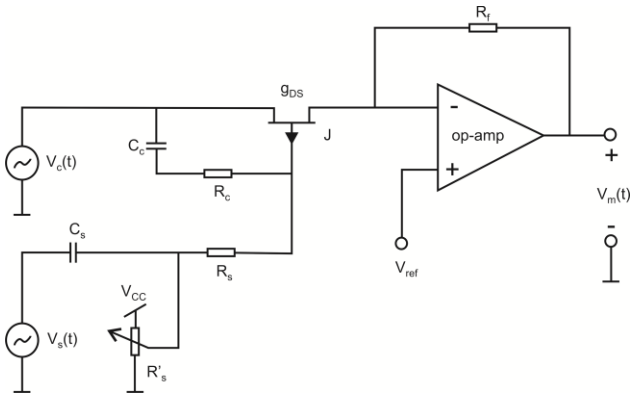

Figure 14. Amplitude modulator circuit using P-channel JFET as voltage variable resistor (VVR). The carrier signal $V_c(t)$ and sound signal $V_s(t)$ will form the amplitude modulated (AM) signal $V_m(t)$.

5. Measurement Set-ups and Results

In bone conduction devices, the input to the microphone is sound pressure and the output is force. Therefore, the performance test of the device can be done by measuring the output force level (OFL) in different sound pressure levels (SPL). To simulate the mechanical impedance of the skull bone a Skull Simulator was used. The Skull simulator generates a voltage proportional to the force applied at the connection point [35]. Measurements were performed in the Brüel & Kjær anechoic test chamber type 4222. A dynamic signal analyzer, Agilent 35670A was employed to generate and analyze signals. Automatic logarithmic swept sine in the frequency range of 100 Hz to 10 kHz was used in all measurements. Linear spectrums of the output force were measured while the input sound pressure kept constant at 60, 70 and 90 dB SPLs with a reference Brüel & Kjær microphone system type 2804. To compare the BCI performance with other bone conduction devices, BAHA Classic 300 and Intenso from Cochlear (Cochlear Bone Anchored Solutions; Mölnlycke, Sweden) and audio processor of the Vibrant Soundbridge from Vibrant MEDEL (Innsbruk, Austria) were used.

Figure 15 shows the OFL of the BCI in 60, 70 and 90 dB SPLs. The 60 dB SPL and 70 dB SPL curves illustrate the

linearity of the device where 10 dB increase in the input sound pressure results in 10 dB increase in the output force. The 90 dB SPL curve is called the Maximum Power Output (MPO) that is the most important output which occurs when the device is saturated and limited by the battery voltage at the output. The shape of the OFL curve is the result of the bone conduction transducer force which has a resonance peak at around 700 Hz. For more details see [14]. Another important measurement of the BCI is to change the coil spacing in the desired range and acquire the MPO curves. The coil spacing is defined as the effective skin thickness. The BCI MPOs in the coil spacing range of 2 mm to 8 mm is depicted in Figure 16.

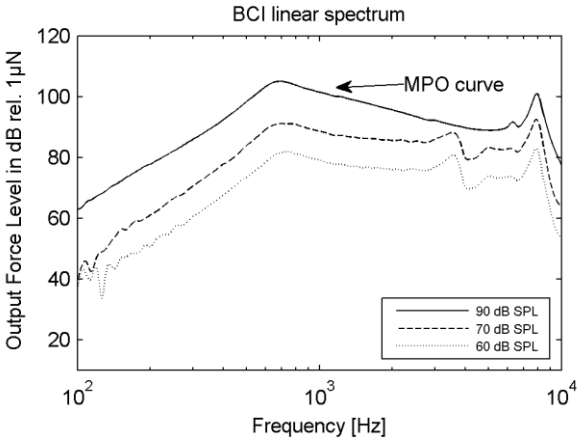

Figure 15. OFL measurements of the BCI in different sound pressure levels (SPLs) at 2 mm coil spacing.

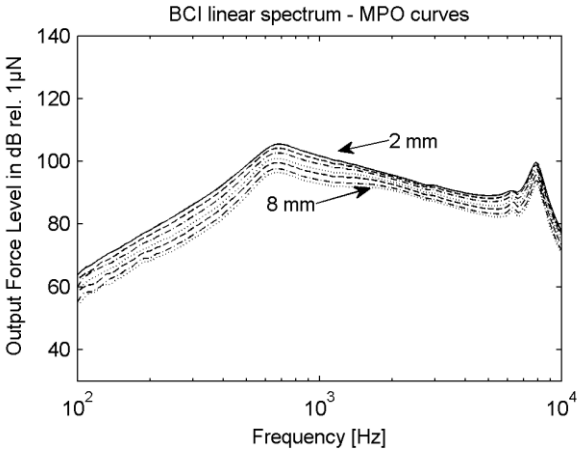

Figure 16. BCI MPOs in different coil spacing.

It is obvious that the maximum output in this design occurs at 2 mm spacing between coils and when the distance increases, the output decreases. For 6 mm changes in the coil spacing, the output decreases nearly 4.9 dB at 2 kHz which maybe can be considered as too much. This can be due to the fact that in the MPO measurements, the AM signal applied to the base of the power amplifier transistor is fairly high and the output transistor operates in saturation that is an extreme undesired condition. At lower input sound pressures the maximum output occurs at 4 mm coil spacing.

Figure 17 presents a comparison of existing bone conduction devices, a middle ear audio processor driving a BCI transducer and the BCI. MPO curves of the BAHA Classic 300, BAHA Intenso and the MEDEL audio processor loaded by the BCI Bone Bridge were measured. 2 mm coil spacing was used in the BCI and MEDEL measurements. Most importantly, the BCI with the analog RF drive can generate the same MPO as the MEDEL device which uses some kind of switching drive. Both devices use RF links that keeps the skin intact whereas the Intenso and Classic 300 are bone anchored devices as they are directly coupled to the bone or Skull Simulator.

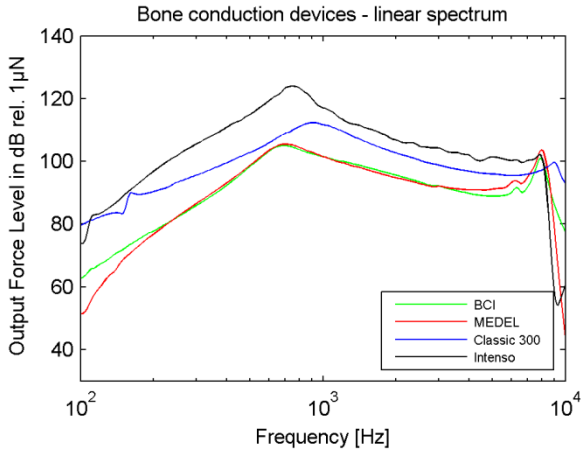

Figure 17. Comparison between bone conduction devices.

Comparing the BCI with Classic 300, it can be concluded that the RF link results in a loss of 10-15 dB in the output force of the device. On the other hand it was shown by Håkansson *et al*. [13-14] that the sensitivity to bone conducted sound increases with the same amount or more when the excitation point of the device moves to a position closer to the cochlea which is the case in the BCI. In this design we have used macro components and current consumption in driver stages has been neglected. However we have noticed that the biasing of the power transistor is power consuming and in a next design a switched topology will be investigated. For future work, to get higher efficiencies and robustness in the link sensitivity, switching topologies such as Class-E and Class-D tuned power amplifiers should be developed. These topologies may also use a series tuned RF link.

6. Conclusions

A new implanted bone conduction device has been developed as an alternative to the percutaneous bone anchored hearing aid. This device which is called the Bone Conduction Implant (BCI) keeps the skin intact. It was found that the BCI device can generate enough output force level that can be used in candidate patients. The BCI

is still sensitive to the spacing that needs a better power amplifier design which prevents saturation of the output transistor.

Acknowledgement(s)

This project was supported by Swedish Governmental Agency for Innovation Systems "VINNOVA".

References

[1] S. Reinfeldt, *Bone Conduction Hearing in Human Communication: Sensitivity, Transmission, and Applications.* (Gothenburg, NJ: Chalmers University of Technology, 2009. Ph.D. Dissertation).

[2] S. Stenfelt, *Acoustic and Physiologic Aspects of Bone Conduction Hearing, Implantable Bone Conduction Hearing Aids.* (Basel, NJ: KARGER, 2011).

[4] B. Håkansson, A. Tjellström, U. Rosenhall, P. Carlsson, The bone-anchored hearing aid: principle design and a psycoacoustical evaluation. *Acta otolaryngol, 100*, 1985, 229-239.

[5] AFM. Snik, EM. Myllanus, C. Cremers, The bone-anchored hearing aid compared with conventional hearing aids. *Otolaryngol Clin North Am, 28,* 1995, 73-78.

[6] B Håkansson, A. Tjellström, G. Granström, The bone-anchored hearing aids-current status in adults and children, *Otolaryngol Clin North Am, 34,* 2001, 337-364.

[7] AFM. Snik, EM. Myllanus, DW. Proops, *et al.*, Consensus statements on the BAHA system: where do we stand at present?, *Ann Otol Rhinol Laryngol Suppl, 195,* 2005,2-12.

[8] A. Tjellström, G. Granström, Long-term follow-up with the bone anchored hearing aid: a review of the first 100 patients between 1977 and 1985, *ENT J, 73,* 1994, 21-3.

[9] RA. Reyes, A. Tjellström, G. Granström. Evaluation of implant losses and skin reaction around extraoral bone anchored hearing implants: a 0- to 8- year follow-up. *Otolaryngol Head Neck Surg, 122,* 2000, 272-6.

[10] RA. Battista, PD. Littlefield. Revision BAHA surgery, *Otolaryngol Clin North Am*, 39, 2006, 801-13.

[11] M. Shirazi, S. Marzo, J. Leonetti. Perioperative complications with the bone anchored hearing aid. *Otolaryngol Head Neck Surg, 134,* 2006, 236-9.

[12] J. Wazen, B. Wycherly, J. Daugherty. *Complications of Bone-Anchored Hearing Devices, Implantable Bone Conduction Hearing Aids.* (Basel, NJ: KARGER, 2011).

[13] B. Håkansson, M. Eeg-Olofsson, S. Reinfeldt , *et al.*, Percutaneous Versus Transcutaneous Bone Conduction Implant system: A Feasibility Study on a Cadaver Head. *Otol Neurotol, 29*, 2008, 1132-1139.

[14] B. Håkansson, S. Reinfeldt, M. Eeg Olofsson, *et al.*, A novel bone conduction implant (BCI): Engineering aspects and pre-clinical studies. *Int J Audiol, 49*, 2010, 203-215.

[15] B. Håkansson, *the Future of Bone Conduction Hearing Devices, Implantable Bone Conduction Hearing Aids.* (Basel, NJ: KARGER, 2011).

[16] M.W. Baker, R. Sarpeshkar, Feedback Analysis and Design of RF Power Links for Low-Power Bionic Systems, *IEEE Transaction on Biomedical Circuits and Systems, 1,* 2007, 28-38.

[17] G. Wang, W. Liu, M. Sivaprakasam, G. Alper Kendir, Design and Analysis of an Adaptive Transcutaneous Power Telemetry for Biomedical Implants, *IEEE Transaction on Circuits and Systems, 52,* 2005, 2109-2117.

[18] K. Goto, T. Nakagawa, O. Nakamura, S. Kawata, An Implantable Power Supply with an Optically Rechargeable Lithium Battery, *IEEE Transaction on Biomedical Engineering, 48*, 2001, 830-833.

[19] H. G. Lim, Y.H. Yoon, C. W. Lee, I. Y. Park, B. S. Song, J. H. Cho, Implementation of a Transcutaneous Charger for Fully Implantable Middle Ear Hearing Device. *27th Conf. IEEE Engineering in Medicine and Biology*, Shanghai, 2005, 6813-6816.

[20] Z. Tang, R.J. Sclabbasi, C. Sun, S.A. Hackworth, *et al*., Transcutaneous Battery Recharging By Volume Conduction and its Circuit Modeling. *28th Conf. IEEE EMBS*, New York, 2006, 644-647.

[21] Z. Hamici, R. Itti, J. Champier, A High-Efficiency Power and Data Transmission System for Biomedical Implanted Electronic Devices. *Meas. Sci. Technol, 7*, 1996, 192-201.

[22] O. Omeni, C. Toumazou, A CMOS Micro-Power Wideband Data/Power Transfer System for Biomedical Implants. *Proc. IEEE Conf. on Circuits and Systems*, 2003, 61-64.

[23] P.R. Troyk, M.A. Schwan. Closed-Loop Class E Transcutaneous Power and Data Link for MicroImplants. *IEEE Transaction on Biomedical Enginnering, 39*, 1992, 589-599.

[25] E.S. Hochmair, System Optimization for Improved Accuracy in Transcutaneous Signal and Power Transmission, *IEEE Transaction on Biomedical Engineering, 31,* 1984, 177-186.

[26] F. Terman, *Radio Engineers' Handbook*, (New York, 1943).

[27] M. Soma, D.C. Galbraith, R.L. White, Radio-Frequency Coils for Implantable Devices: Misalignment Analysis and Design Procedure, *IEEE Transaction on Biomedical Engineering, 34*, 1987, 276-282.

[28] C.M. Zierhofer, E.S. Hochmair, Geometric Approach for Coupling Enhancement of Magnetically Coupled Coils, *IEEE Transaction on Biomedical Engineering, 43*, 1996, 708-714.

[29] N. Donaldson, T.A. Perkins, Analysis of Resonant Coupled Coils in the Design of Radio Frequency Transcutaneous links. *Medical and Biological Engineering and Computing, 21,* 1983, 612-627.

[30] W.H. Ko, S.P. Liang, C. Fung, Design of Radio-Frequency Powered Coils for Implant Instruments, *Medical & Biological Engineering & Computing, 15,* 1977, 634-640.

[31] D.C. Galraith, M. Soma, R.L. White, A Wide-Band Efficient Inductive Transdermal Power and Data Link with Coupling Insensitive Gain, *IEEE Transaction on Biomedical Engineering, 344*, 1987, 265-275.

[34] B. Håkansson, The balanced electromagnetic separation transducer: A new bone conduction transducer, *Journal of Acoustical Society of America, 113*, 2003, 818-825.

[35] B. Håkansson, P. Carlsson, Skull simulator for direct bone conduction hearing devices. *Scandinavian Audiology, 18*, 1989, 91-98.